Lessons from Nanoscience: A Lecture Note Series
ISSN: 2301-3354

"Lessons from Nanoscience" aims to present new viewpoints that help understand, integrate, and apply recent developments in nanoscience while also using them to re-think old and familiar subjects. Some of these viewpoints may not yet be in final form, but we hope this series will provide a forum for them to evolve and develop into the textbooks of tomorrow that train and guide our students and young researchers as they turn nanoscience into nanotechnology. To help communicate across disciplines, the series aims to be accessible to anyone with a bachelor's degree in science or engineering.

More information on the series as well as additional resources for each volume can be found at: http://nanohub.org/topics/LessonsfromNanoscience

Published:

Vol. 1 Lessons from Nanoelectronics: A New Perspective on Transport
by Supriyo Datta

Vol. 2 Near-Equilibrium Transport: Fundamentals and Applications
by Mark Lundstrom, Changwook Jeong and Raseong Kim

Vol. 3 Thermal Energy at the Nanoscale
by Timothy S Fisher

Lessons from Nanoscience:
A Lecture Note Series
Vol. 3

THERMAL ENERGY AT THE NANOSCALE

Timothy S Fisher

Purdue University, USA

World Scientific

NEW JERSEY • LONDON • SINGAPORE • BEIJING • SHANGHAI • HONG KONG • TAIPEI • CHENNAI

temperatures the low-frequency scattering rate is fixed by the defect scattering term. However, for the higher temperatures, the U process scattering rate steadily overtakes the defect rate as frequency increases, leading to a large increase that dominates the effective scattering rate for almost all frequencies. Only at the lowest temperature is defect scattering significant.

The effect of temperature can be further understood through the variation of thermal conductivity as shown in Fig. 5.10 (which assumes a constant group velocity of $v_g = 1000$ m/s for simplicity). The thermal conductivity is calculated using Eq. (5.7):

$$\kappa = \frac{1}{2\pi}\int_0^\infty \Lambda(\omega) M_{dD}(\omega)\hbar\omega \frac{\partial f^o_{BE}}{\partial T} d\omega$$

$$(1D) = \frac{1}{2\pi}\int_0^\infty \frac{v_g}{\tau^{-1}(\omega)}\hbar\omega \frac{\partial f^o_{BE}}{\partial T} d\omega. \qquad (5.30)$$

In Fig. 5.10 the thermal conductivity for temperatures below 10 K inherits the characteristic temperature dependence of the specific heat ($c_v \sim T^1$ for this 1D example). Thereafter, a transition occurs in which the temperature dependence becomes dominated by U process scattering ($\tau_U^{-1} \sim T$) while the specific heat begins to asymptote toward a constant value (according to the Law of Dulong and Petit). As temperature increases further, the scattering rate continues to increase, resulting is a pronounced decrease in thermal conductivity. This simple example illustrates qualitatively the typical regimes of a material whose thermal conductivity is dominated by phonons:

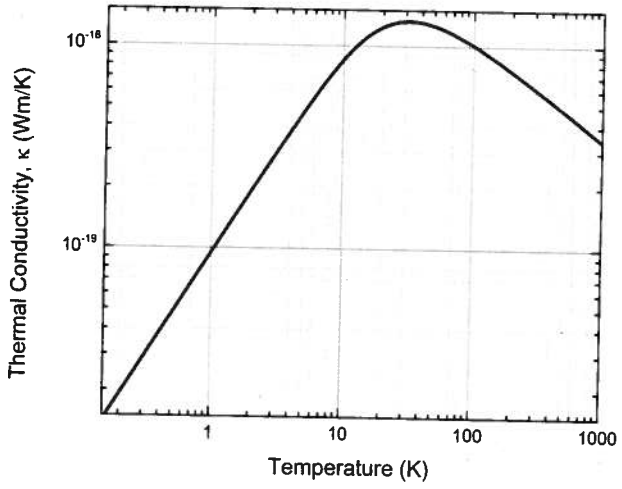

Fig. 5.10 Thermal conductivity of a 1D material as a function of temperature for the example of combined defect and U process scattering. The region below $T = 10$ K is dominated by defect scattering. Above 10 K, U scattering and the plateauing of specific heat with temperature become prominent.

- Increasing thermal conductivity with increasing cryogenic temperatures dominated by the material's specific heat.
- A range of transition temperatures in which the increase in specific heat begins to moderate while phonon-phonon scattering becomes prevalent. The peak thermal conductivity occurs in this region.
- A decreasing thermal conductivity at high temperatures as specific heat becomes constant while the phonon-phonon scattering rate continues to increase.

5.6 Interfacial Transmission

Individual nanomaterials can exhibit extreme thermal properties—both high and low magnitudes. In applications such as thermal insulation or thermoelectrics, the objective is to suppress heat conduction, and a common strategy is to introduce numerous heterogeneous material interfaces that reflect thermal energy carriers. At the other extreme, the engineering objective is typically to translate the outstanding thermal properties of *individual* nanoscale elements to more practical human length scales by connecting many (typically billions) such elements to each other and to the 'bulk' contacts of the real world. Achieving such a circumstance is, however, made very difficult because of the many local interfaces whose presence often mutes the very properties for which the nanoscale elements were chosen. In both cases—high and low property extremes—an understanding of heat flow across interfaces is essential.

Interfacial heat flow is often quantified by its *thermal boundary (interface) resistance*[3] or its inverse, the thermal boundary conductance. Using

[3] For solid-fluid interfaces, the resulting resistance is often called the Kapitza resistance Kapitza (1941).

our prior framework, the expression for thermal boundary resistance is:

$$R_b = \frac{T_1 - T_2}{Q_{\text{ph}}}$$

$$= \frac{T_1 - T_2}{\sum_p \frac{1}{2\pi} \int_0^\infty \hbar\omega M(\omega)\mathcal{T}(\omega)\left[f^o_{BE}(T_1) - f^o_{BE}(T_2)\right] d\omega} \tag{5.31}$$

$$\approx \left[\sum_p \frac{1}{2\pi} \int_0^\infty \hbar\omega M(\omega)\mathcal{T}(\omega)\frac{\partial f^o_{BE}}{\partial T} d\omega\right]^{-1}, \tag{5.32}$$

where the latter approximation derives from $\Delta T \to 0$. The area-normalized resistance becomes:

$$R_b'' = R_b \times \text{'area'} \approx \left[\sum_p \frac{1}{2\pi} \int_0^\infty \hbar\omega M_{dD}(\omega)\mathcal{T}(\omega)\frac{\partial f^o_{BE}}{\partial T} d\omega\right]^{-1}. \tag{5.33}$$

The challenge is therefore to evaluate the transmission function $\mathcal{T}(\omega)$, as developed in the following subsections for smooth (acoustic mismatch) and rough (diffuse mismatch) interfaces.

5.6.1 *Acoustic Mismatch*

We begin the study of interfaces with the continuum version the 1D atomic chain. Consider a two-segment string that is stretched under a fixed tension T_e as shown in Fig. 5.11. A wavefront of arbitrary displacement form f_1 is incident rightward from string 1 on the interface, and the wave then partially reflects (g displacement) and transmits into string 2 (f_2 displacement). Basic acoustic theory (French, 1971) reveals that the acoustic velocity in a string can be expressed as:

$$v_a = \sqrt{\frac{T_e}{\mu}}, \tag{5.34}$$

where μ is the mass density of the string (mass per unit length).

The transverse displacements (y_1 and y_2) in each string can be expressed as:

$$y_1(x,t) = f_1\left(t - \frac{x}{v_1}\right) + g\left(t + \frac{x}{v_1}\right),$$

$$y_2(x,t) = f_2\left(t - \frac{x}{v_2}\right), \tag{5.35}$$

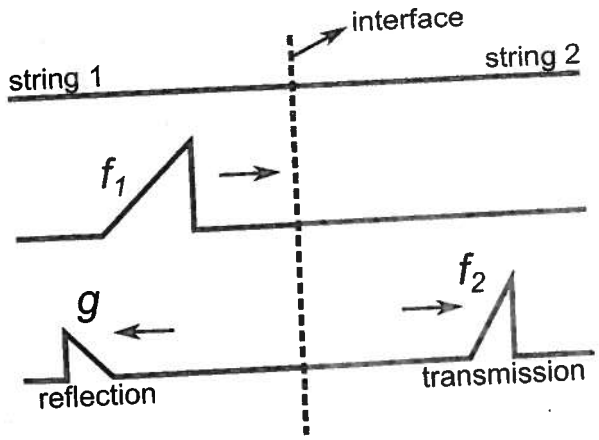

Fig. 5.11 Reflection and transmission of a wave on strings under tension. The wave is partially reflected and transmitted at the interface, where a discontinuity in mass density μ exists.

with boundary conditions:

$$y_1(0,t) = y_2(0,t), \tag{5.36}$$

$$\frac{\partial y_1}{\partial x}(0,t) = \frac{\partial y_2}{\partial x}(0,t). \tag{5.37}$$

Using the interface conditions ($x = 0$) to solve for f_2 and g in terms of f_1 reveals:

$$f_2(t) = \frac{2v_2}{v_2 + v_1} f_1(t) \tag{5.38}$$

$$g(t) = \frac{v_2 - v_1}{v_2 + v_1} f_1(t) \tag{5.39}$$

From the foregoing relations, we can solve for the reflected displacement in terms of the transmitted displacement:

$$g(t) = \frac{v_2 - v_1}{2v_2} f_2(t). \tag{5.40}$$

These relations lead to the following intuitive observations:

- If $v_1 = v_2$, then nothing is reflected (all transmitted)
- If $v_2 = 0$ (infinite mass), then all is reflected

To this point, we have considered displacements (y, f, g) and velocities (v_a), but our prime focus is energy, specifically the rate of energy flow (French, 1971):

$$P = \frac{1}{2}\mu y_{\max}^2 v_a \omega^2, \tag{5.41}$$

where $y_{\max}$ is the peak displacement, and ω is the frequency of oscillation.

The ratio of power reflected at the interface to that incident becomes:

$$\frac{P_g}{P_{f1}} = \left(\frac{g}{f_1}\right)^2 = \left(\frac{v_2 - v_1}{v_2 + v_1}\right)^2. \tag{5.42}$$

Instead of velocities, the concept of *acoustic impedance* (Z) is often used:

$$Z = \frac{T_e}{v_a} = \sqrt{T_e \mu} = \mu v_a. \tag{5.43}$$

Then, the normal-direction interfacial energy transmittance from string 1 to string 2 (t_{12}) becomes:

$$t_{12} = 1 - \left(\frac{g}{f_1}\right)^2 = 1 - \left(\frac{Z_1 - Z_2}{Z_1 + Z_2}\right)^2 = \frac{4Z_1 Z_2}{(Z_1 + Z_2)^2}. \tag{5.44}$$

Expressed in terms of velocity, the transmittance is:

$$t_{12} = \frac{4v_1 v_2}{(v_1 + v_2)^2}. \tag{5.45}$$

Note that the reverse transmittance t_{21} from string 2 to string 1 is mathematically identical to t_{12} due to the symmetry of the result. This model is called the Acoustic Mismatch Model (AMM) (Little, 1959).

We turn our attention back to the contact-device-contact arrangement to understand the effects of an internal interface within the device as shown in Fig. 5.12. Our prior derivations presumed a uniform number of modes (M) in the device:

$$Q_{\text{ph}} = \frac{1}{2\pi}\int_0^\infty M(\omega)\mathcal{T}(\omega)\hbar\omega\left[f_{BE}^o(T_1) - f_{BE}^o(T_2)\right] d\omega. \tag{5.46}$$

What happens if M changes from one side of the device to the other? For such situations, we must use the concept of interfacial energy transmittance that is specific to a given direction (e.g., t_{12} in Eq. (5.44)).

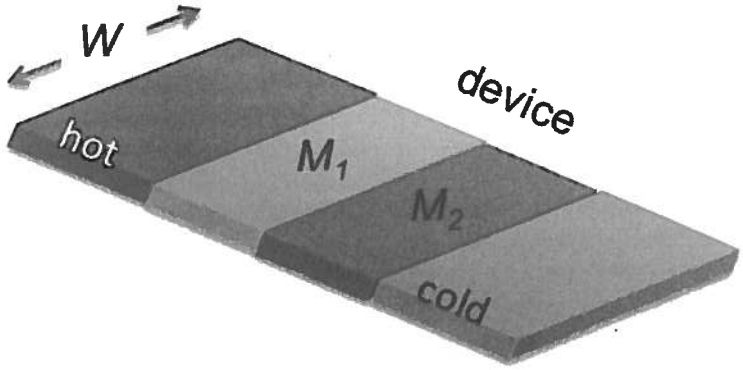

Fig. 5.12 Schematic of a contact-device-contact arrangement in which the number of modes changes at an interface within the device.

The form of Eq. (5.54) that allows for mode discontinuity and direction-specific transmission is:

$$Q_{\text{ph}} = \frac{1}{2\pi}\int_0^\infty \hbar\omega\left[M_1(\omega)t_{12}(\omega)f_{BE}^o(T_1) - M_2(\omega)t_{21}(\omega)f_{BE}^o(T_2)\right] d\omega. \tag{5.47}$$

As a reminder, the number of modes is:

$$M_i(\omega) = \text{'area'} \times \pi \langle v_{g,x} \rangle D_{dD}(\omega), \tag{5.48}$$

where i denotes the side of the device. The *principle of detailed balance* requires that the integral in Eq. (5.47) must be zero when the two contact temperatures are the same, $T_1 = T_2$. Consequently, the number of modes and transmittances must be related by:

$$M_1(\omega)t_{12}(\omega) = M_2(\omega)t_{21}(\omega) = M_i(\omega)\mathcal{T}_i(\omega). \tag{5.49}$$

This result indicates that the number of modes and transmittance should be thought of as a collective entity for problems in which the number of modes changes across an interface. Moreover, the transmittance itself can depend on the direction of the carrier, in which case the spatial averaging used previously to define the number of modes must be revisited (see Eqs. (4.3)–(4.6) and Eqs. (4.23)–(4.25)).

Extension of the AMM beyond the 1D analysis above provides an example for the process of directional averaging. The multi-dimensional version

of the AMM is Little (1959):

$$t_{12}(\theta_1,\omega) = t_{21}(\theta_2,\omega) = \frac{\frac{4Z_2}{Z_1}\cdot\frac{\cos\theta_2}{\cos\theta_1}}{\left(\frac{Z_2}{Z_1}+\frac{\cos\theta_2}{\cos\theta_1}\right)^2}, \tag{5.50}$$

where θ_1 and θ_2 are the incident and transmitted (refracted) polar angles, as shown in Fig. 5.13. Any frequency dependence in the transmittances would be manifested in the velocity terms that comprise the acoustic impedances and the refracted angle θ_2, although most often the Debye approximation is used in conjunction with the AMM. The incident and transmitted angles are related by Snell's law:

$$\sin\theta_2 = \frac{v_{g2}}{v_{g1}}\sin\theta_1. \tag{5.51}$$

The directional dependence of t_{xy} necessitates a revisiting of the **k**-space integral expression for heat flow rate. The 3D version can be expressed as:

$$\begin{aligned} Q_{ph} &= \frac{\text{'area'}}{8\pi^3}\int_0^{2\pi}\int_0^{\frac{\pi}{2}}\int_0^{\infty}\hbar\omega\begin{bmatrix} t_{12}(\theta,\omega)v_{g1}\cos\theta\sin\theta f^o_{BE}(T_1) \\ -t_{21}(\theta,\omega)v_{g2}\cos\theta\sin\theta f^o_{BE}(T_2)\end{bmatrix}k^2 dk d\theta d\psi \\ &= \frac{\text{'area'}\pi}{2\pi}\int_0^{\frac{\pi}{2}}\int_0^{\infty}\hbar\omega\begin{bmatrix} t_{12}(\theta,\omega)v_{g1}\cos\theta\sin\theta D_{1,3D}(\omega) f^o_{BE}(T_1) \\ -t_{21}(\theta,\omega)v_{g2}\cos\theta\sin\theta D_{2,3D}(\omega) f^o_{BE}(T_2)\end{bmatrix}d\omega d\theta, \end{aligned} \tag{5.52}$$

where $D_{i,3D}(\omega)$ is the 3D phonon density of states for side i.

The principle of detailed balance requires that the directional (θ) integral over the bracketed term in Eq. (5.52) must be zero when $T_1 = T_2$ (i.e., when $f^o_{BE}(T_1) = f^o_{BE}(T_2)$). Therefore, the following relation must hold:

$$\begin{aligned} &\text{'area'}\pi\left[\int_0^{\frac{\pi}{2}} t_{12}(\theta,\omega)v_{g1}\cos\theta\sin\theta d\theta\right]D_{1,3D}(\omega) \\ &= \text{'area'}\pi\left[\int_0^{\frac{\pi}{2}} t_{21}(\theta,\omega)v_{g2}\cos\theta\sin\theta d\theta\right]D_{2,3D}(\omega) \\ &\equiv \overline{\mathcal{T}}(\omega), \end{aligned} \tag{5.53}$$

where the final equivalence defines a directionally averaged product of the number of modes and transmission function. This function can be used in

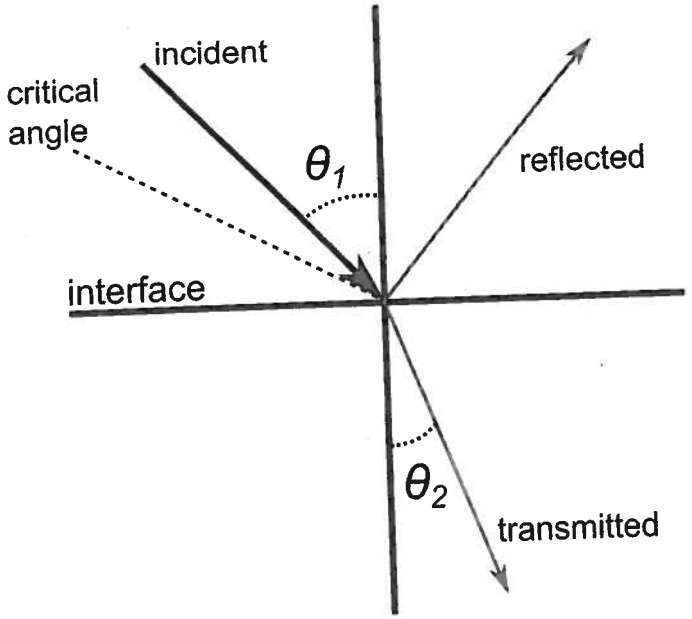

Fig. 5.13 Multi-dimensional reflection and refraction of phonons at an interface under acoustic mismatch. The refraction follows Snell's law.

the general expression for heat flow rate as:

$$\begin{aligned} Q_{\text{ph}} &= \frac{1}{2\pi}\int_0^{\infty}\overline{\mathcal{T}}(\omega)\hbar\omega\left[f^o_{BE}(T_1) - f^o_{BE}(T_2)\right]d\omega \\ Q_{\text{ph}} &= \frac{1}{2\pi}\int_0^{\infty} M_i(\omega)\mathcal{T}_{AMM,i}(\omega)\hbar\omega\left[f^o_{BE}(T_1) - f^o_{BE}(T_2)\right]d\omega, \end{aligned} \tag{5.54}$$

where the last equality involves a definition of an effective transmission function for the AMM:

$$\mathcal{T}_{AMM,i}(\omega) \equiv \frac{\overline{\mathcal{T}}(\omega)}{M_i(\omega)}. \tag{5.55}$$

Here, the denominator is the previously defined 'number of modes' (see Eq. (5.48)).

The foregoing development reveals a subtle but important observation—namely, that the density of states of only *one* side of the interface needs to be known in order to solve for the overall transport rate. This finding is also observable from Eq. (5.49) for problems with a difference in

the number of modes but directionally independent transmittance and is a general consequence of the principle of detailed balance.

The actual function $\overline{T}(\omega)$ for the AMM and other models is complicated because it involves a combination of the directional dependence of Eq. (5.50) and Snell's law (Eq. (5.51)). Little (1959) and Cheeke (1976) used a related functional:[4]

$$\Gamma(\omega) = \int_0^{\frac{\pi}{2}} t_{12}(\theta,\omega)\cos\theta\sin\theta d\theta = \frac{\overline{T}(\omega)}{\text{'area'}\pi D_{1,3D} v_{g1}}$$
$$= \frac{\overline{T}(\omega)}{2M_1} = \frac{1}{2}\mathcal{T}_{AMM,1}(\omega), \tag{5.56}$$

where the frequency dependence of the transmission is retained for generality. We note that any frequency dependence of the foregoing expression would be contained in the transmittance (t_{12}). However, under the Debye approximation, the velocities are assumed constant, and this frequency dependence disappears. Tabulated values of Γ for the AMM under the Debye approximation have been provided by Cheeke *et al.* (1976) for parameterized acoustic impedances. Instead of a plot of Γ, we include here a contour graph of the average AMM transmission function $\mathcal{T}_{AMM}$ in Fig. 5.14.

5.6.2 *Diffuse Mismatch*

A fundamentally different but also commonly used interface transmission theory is called the Diffuse Mismatch Model (DMM). The term 'diffuse' implies randomness (or something 'spread out'), and in diffuse interface scattering a phonon loses the memory of its origin and its type (branch). In this sense, the DMM can be considered the opposite extreme of the AMM, which generally presumes a retention of phonon coherence. This model applies particularly well to interfaces that are rough in comparison to the carrier wavelength (cf., Fig. 5.2). A carrier moving away from a diffuse interface 'forgets' its original location and branch, and as a result, the transmittance into a particular side is equivalent to reflectance from that side back into itself:

$$t_{12} = r_{21} = 1 - t_{21}, \tag{5.57}$$

[4]Note that their term $\alpha_1(\theta)$ is equivalent to $t_{12}(\theta)$ used here.

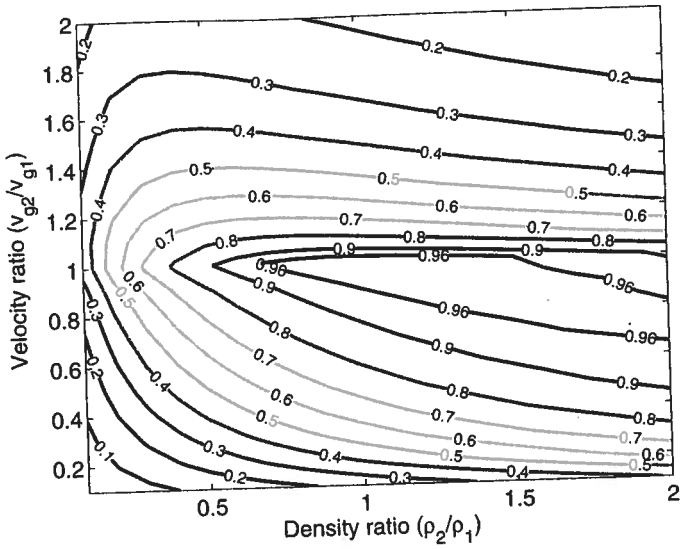

Fig. 5.14 Average AMM transmission coefficient for different group velocities and density ratios.

where the second equality derives from an energy balance (a carrier must be either transmitted or reflected—nothing is absorbed by assumption). The transmittances and reflectances are shown schematically in Fig. 5.15.

Because a scattered phonon can proceed, by assumption, into any branch that is active at its frequency (energy), the summation over branches[5] must be included in the statement of detailed balance that is applicable to the DMM:

$$\sum_p M_1(\omega)t_{12}(\omega) = \sum_p M_2(\omega)t_{21}(\omega) = \sum_p M_2(\omega)\left[1 - t_{12}(\omega)\right]. \tag{5.58}$$

The transmittance does not depend on branch, and therefore, it can be solved as:

$$t_{12}(\omega) = \frac{\sum_p M_2(\omega)}{\sum_p M_1(\omega) + \sum_p M_2(\omega)}. \tag{5.59}$$

[5]We have avoided including the branch summations where it is not essential in prior derivations, for the sake of clarity.

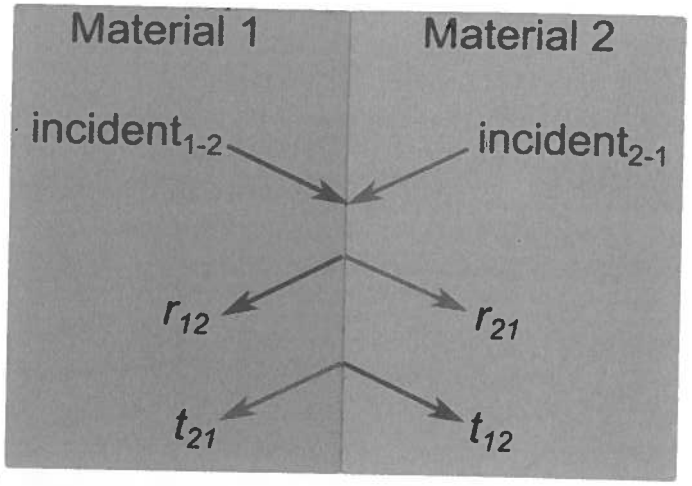

Fig. 5.15 Reflection and transmission at a material interface. If the process is diffuse, then $t_{ij} = r_{ji}$.

The foregoing expression gives the important result that the DMM transmittance is proportional to the fraction of total modes (sides 1 and 2) available on the opposite side of the interface.

$$\boxed{M_1(\omega)\mathcal{T}_1(\omega) = M_1(\omega)\frac{\sum\limits_p M_2(\omega)}{\sum\limits_p M_1(\omega) + \sum\limits_p M_2(\omega)}}. \tag{5.60}$$

5.7 Thermionic Electron Emission

As stated previously, electron transport is also critically important to heat conduction in bulk metals. Further, coupled electrical-thermal transport is dispositive in determining the performance of many technologically important devices, such as solid-state transistors and thermoelectric materials. Much of the foundational theory associated with the transport of heat by electrons can be obtained from other books in this series by Datta (2012), and Lundstrom and Jeong (2013), particularly when viewed through analogies such as the Wiedemann-Franz law. Here, we focus on the topic of thermionic electron emission through the perspective of modes and transmission developed above. Thermionic transport, while perhaps less common than the ubiquitous transistor, plays a critical role in applications such as electron sources for imaging instruments (e.g., scanning electron microscopes) and in both vacuum (Hatsopoulos and Gyftopoulos, 1973) and solid-state (Shakouri and Bowers, 1997) thermal-to-electrical energy conversion processes.

We begin with a general description of electron emission processes. Figure 5.16 illustrates two possible electron emission pathways from a solid metal into vacuum. Electrons can emit over potential barriers (thermionic emission), or they can tunnel through them (field emission). Field emission involves quantum tunneling through a triangular potential barrier formed by the application of an electric field between the two electrodes (i.e., cathode and anode). Fowler and Nordheim (1928) developed the first theory

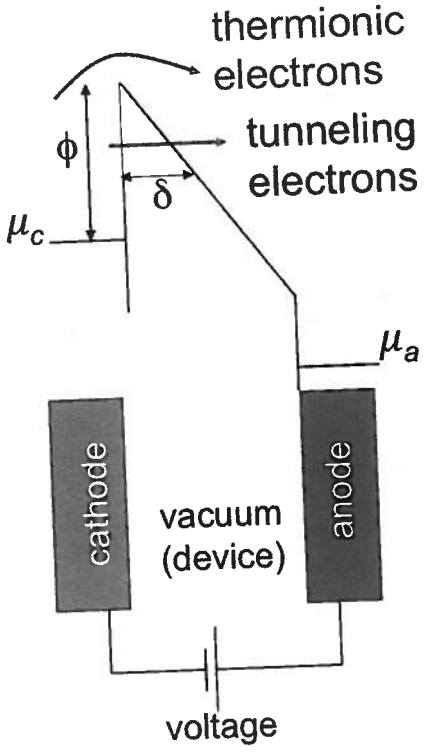

Fig. 5.16 Schematic of thermionic and field electron emission. The power supply creates an electric field through which field-emitted electrons tunnel. Thermionic electrons emit over the energy barrier entirely.